Journal of Nuclear Materials 581 (2023) 154455

Contents lists available at ScienceDirect

Journal of Nuclear Materials

journal homepage: www.elsevier.com/locate/jnucmat

Deuterium retention in tungsten, tungsten carbide and tungsten-ditungsten carbide composites

P. Jenuš [a,*], A. Abram [a], S. Novak [a,b], M. Kelemen [a,b], M. Pečovnik [a], T. Schwarz-Selinger [c], S. Markelj [a]

[a] Jožef Stefan Institute, Jamova c. 39, 1000 Ljubljana, Slovenia
[b] Jožef Stefan International Postgraduate School, Jamova c. 39, 1000 Ljubljana, Slovenia
[c] Max-Planck-Institut für Plasmaphysik, Boltzmannstrasse 2, D-85748 Garching, Germany

HIGHLIGHTS

- Deuterium retention was studied in three systems: pure W, W-W_2C composite, and WC with some additional carbon.
- The highest d retention was measured in W-W_2C composite.
- Formation of blisters and pillars was observed in pure w and in W-W_2C composite, but not in the WC.

ARTICLE INFO

Keywords:
Tungsten
(di)tungsten carbide
Deuterium
NRA
TDS

ABSTRACT

The selection of the most suitable material for the EU DEMO divertor is still underway. Current research focuses on the development of tungsten-based materials for plasma-facing applications. In addition to other requirements, the candidate material must also exhibit low intrinsic hydrogen isotope retention. To verify the suitability of the tungsten carbide-containing materials, we examined the effect of carbon in the form of carbide or free carbon on deuterium (D) retention.

The samples were consolidated by Field Assisted Sintering (FAST) and examined in terms of phase composition and microstructure before the D-retention studies. The Nuclear Reaction Analysis (NRA) technique was used to determine the depth distribution of D after the exposure to D plasma (fluence of 1.3×10^{24} D/m^2 and 1.3×10^{25} D/m^2 and an exposure temperature of 370 K and 523 K, respectively). Thermal Desorption Spectroscopy (TDS) was used to measure the D desorption spectra. The surfaces of samples exposed to D plasma were also examined in terms of microstructure by scanning electron microscopy. The study has shown that apart from the D-fluence and exposure temperature, the materials' composition plays a vital role in D-retention, accompanied by blisters and pillar formation. The lowest D-retention was observed for tungsten and the highest in the W-W_2C composite. The blisters and pillars were formed in these two materials but not in the WC, which also contains free carbon. At higher D fluence, approximately 15 to 20-times more blisters and pillars were formed in the W-W_2C composite than in the tungsten prepared by the same method. The results suggest that the number of defects causing higher D-retention is the highest in W-W_2C. On the other hand, the absence of surface irregularities in the WC-C sample after D retention studies indicates that the cause for higher D retention does not lie in the carbides, but, presumably, the microstructural and crystal lattice defects govern the D retention in tungsten-tungsten carbide systems.

1. Introduction

The development and implementation of fusion power plants promise a significant contribution to a clean and safe energy supply for future generations. To ensure their high efficiency and safe operation, extensive efforts are being put into developing structural materials capable of withstanding the extreme conditions in the reactor. Such as high energy neutron bombardment and hydrogen isotope ion exposure,

* Corresponding author.
E-mail address: petra.jenus@ijs.si (P. Jenuš).

https://doi.org/10.1016/j.jnucmat.2023.154455
Received 11 November 2022; Received in revised form 7 April 2023; Accepted 15 April 2023
Available online 16 April 2023

combined with high thermal flux and continuous production of helium (He) through (n, p) and (n, α) nuclear reactions in plasma-facing components (PFCs; first wall and divertor). Within the European demonstration power plant (EU DEMO) design, the essential task is to select suitable material for the divertor, which is a critical in-vessel component. The divertor is responsible for heat transfer and impurity removal via a guided plasma exhaust and is, therefore, subjected to very high heat fluxes. Although recent decades have seen substantial progress in the field of fusion-relevant materials, developing improved materials remains amongst the priorities of fusion research programmes. The goal is to prepare a low-activation material capable of withstanding high heat loads of more than 10 MW/m^2, with sufficient mechanical and thermal properties retained even after high neutron irradiation dose and nuclear transmutations [1–3]. In addition, the material must also exhibit low intrinsic hydrogen isotope retention [4]. The latter is especially important as high levels of radioactive tritium retention in the material could lead to a fuel-inefficient fusion tokamak operation and other health and safety risks. Furthermore, such an issue could be promoted even further by the material lattice displacement damage created throughout the material by 14 MeV fusion neutrons, as the presence of displacement damage has been shown to increase hydrogen isotope (HI) retention by orders of magnitude [5,6].

Tungsten (W) and tungsten with transition-metal ceramic particles show high thermal conductivity and high melting point [1,7–9]. Rolled W was chosen in the ITER due to the low hydrogen isotope retention [10], but current research focuses on developing tungsten-based materials as pure W deteriorates under operating conditions of the EU DEMO reactor [2,11]. The currently proposed solutions for the structural stabilisation of tungsten include particle reinforcement by incorporating oxide (e.g. Y_2O_3) or carbide (e.g. TiC, TaC and W_2C) particles into the W matrix that improves the material's mechanical properties to a certain extent [12–18]. On the other hand, it is known that various defects can act as HI trapping sites, which implies that microstructure affects D-retention in W-materials. Different types and densities of lattice imperfection, such as dislocations, impurities and vacancies produced by different material manufacturing techniques, result in different surface morphology and microstructure feature (such as inclusions, pores, grain structure and grain boundaries). Thus, not only the composition of the material but also its microstructure has to be considered. In this work, we present and discuss three types of FAST-consolidated fusion-relevant W-based materials to verify the effect of tungsten carbide inclusions on deuterium retention.

2. Experimental

2.1. Sample preparation

Starting powders used in this study were tungsten powder (average grain size of $\leq$ 1.5 μm, Global Tungsten & Powders spol. S r.o., Czech Republic), tungsten carbide powder (WC with an average grain size of 150–200 nm, >99%, Aldrich, Germany) and graphene flakes (60 nm flakes, Grade AO-4, Graphene Supermarket, USA). Powders were mixed according to ratios presented in Table 1, producing three different sets of samples. The homogenisation was ensured by dispersing powders in cyclohexane (Sigma Aldrich, Germany), followed by homogenisation with an ultrasonic processor VCX500 (Sonics & Materials Inc., USA) freeze-drying. The powder mixtures were sintered in a graphite die with an inner diameter of 10 mm using field-assisted sintering (FAST, Dr Sinter FAST 515-S, Sumimoto FAST Syntex Ltd., Japan) at either 1700 °C (samples WC—C) or 1900 °C (samples W and W-W_2C) with a heating rate of 100 °C/min, for 5 min and under an applied uniaxial pressure of 60 MPa. A protective foil was used to separate the powders, and the graphite die during powder consolidation. Two types of foil were used: in the case of W and W-WC powder mixture, tungsten foil was used, and in the case of WC—C, graphite foil was applied. Before the FAST processing, the reaction chamber was purged several times with high-purity argon and evacuated again. During sintering, the pressure inside the chamber was below 10 Pa.

As-sintered samples were polished, analysed in terms of phase composition and microstructure and then subjected to D-retention studies. Two sets of samples were exposed to a well-defined low-temperature D plasma (PlaQ) [19]. The ion flux consists mainly of D_3^+ ions with a 3% contribution of D^+ and D_2^+. At a bias voltage of 100 V, the corresponding ion energy was 38 eV/D. The implantation D ion flux at these conditions was 1.25×10^{20} D/m^{2}s. Samples were exposed at 370 K for 3 h and 30 h corresponding to a D ion fluence of 1.35×10^{24} D/m^2 and 1.35×10^{25} D/m^2, respectively. The same set of samples was re-polished after an analysing procedure and exposed to the same low-temperature D plasma at a higher sample temperature of 523 K as compared to the first exposure set for 30 h yielding fluence of 1.35×10^{25} D/m^2. Three different samples were mounted in each batch, and D-plasma was exposed simultaneously to ease the comparison of experimental results. After the D plasma exposure, the resulting D depth profiles were measured using the Nuclear Reaction Analysis (NRA) technique. To complete the analysis of D retention, the D desorption spectrum was measured for the large fluence set of samples using Thermal Desorption Spectroscopy (TDS).

2.2. Characterisation

Before the analysis, the outer layer of the sintered material was removed by grinding. The phase composition of the sintered samples was analysed by X-ray diffraction (XRD; AXS U8, Bruker Co., USA) utilising Cu–Kα radiation at room temperature (step width of 0.02°, fixed time of 1 s, a scanning range of $2\theta = 20°$ to 80°). A Rietveld analysis was performed using the programme package Topas, Bruker AXS, Karlsruhe, Germany. Before and after D irradiation, the microstructure of consolidated samples was characterised by scanning electron microscopy (SEM) (FE-SEM, JSM-7600F, Jeol Inc., Japan and Helios NanoLab 650, FEI, US). The grain size distribution was obtained from a planimetric analysis conducted on four SEM micrographs per sample, considering $\geq$ 500 grains using image-analysis software (ImageJ). Additionally, for the sample W-W_2C the grain size was also determined by EBDS analysis.

The relative density of sintered pellets was calculated from geometrical density, considering that the theoretical density of pure W is 19.25 g/cm^3, of pure WC is 15.7 g/cm^3, and 17.1 g/cm^3 for pure W_2C, respectively.

The Nuclear Reaction Analysis (NRA) technique allowed the determination of the depth distribution of D after exposure to D plasma. The nuclear reaction D(^{3}He, α)p was used to determine the D depth profile. The ^{3}He analysing beam was 2 mm in diameter. Six analysing beam energies ranged from 0.7 MeV to 4.2 MeV. The chosen set of analysing energies allows us to probe the D depth profile to a maximum depth of

Table 1
Composition of the samples and as-consolidated relative densities.

Sample	The concentration of added carbon in the starting mixture (at.%)	Composition after sintering determined by Rietveld refinement analysis (in wt%)	Relative density (%)
1: W	3.7	100% W	95.3 ± 0.5
2: W-W_2C	7.2	96± 1% *W* + 4 ± 1% W_2C	98.4 ± 1
3: WC—C	2	93± 1% WC + 7 ± 1% C	98.6 ± 0.3

around 7 μm. A PIPS detector with a solid angle of 26.7 msr was used to measure the energy spectrum of the protons coming from the D(^{3}He, α)p reaction. A second PIPS detector was positioned at 165° scattering angle to detect the Rutherford backscattered projectile (RBS) particles and is used primarily for dose calibration of the NRA measurement. The raw proton energy spectra measured with the NRA technique were input into NRADC [20], which outputs the optimised D depth profile.

The D desorption spectra were measured using Thermal Desorption Spectroscopy (TDS). The TDS measurement was performed in the TESS set-up at IPP using a linear heating ramp of 3 K/min up to 1010 K and *a* > 30 min hold at the highest temperature. The calibration of D_2 was performed with a D_2 leak with a leak rate of 1.2234×10^{14} D_2 molecules/*sec*. The calibration factor for HD was determined by flowing HD through an orifice of known size from a calibrated volume of known absolute pressure (measured with a capacitance manometer and spinning rotor gauge) into the mass spectroscopy vessel. To determine the amount of D desorbed during the measurement, masses 3 amu/q and 4 amu/q, corresponding to HD and D_2 molecules, respectively, were summed up. The amount of D desorbed in other species like D_2O was negligible. The sample temperature during the TDS measurement was monitored directly using a shielded thermocouple in direct contact with the sample. For more details on the TDS measurement, please see Ref. [21].

3. Results & discussion

3.1. Characteristics of the as-consolidated samples

The as-synthesised samples were first characterised in terms of phase composition and microstructure. We examined three types of samples: 1) tungsten without secondary phases, 2) W-W_2C composite and 3) WC with free carbon remains. The as-consolidated samples were first characterised in terms of phase composition and microstructure.

The XRD analysis spectra are shown for all samples in Fig. 1a. From the XRD analysis of the FAST consolidated sample W, prepared from W with the addition of 3.7 at.% of carbon in the form of WC nanoparticles, only tungsten was detected (see Table 1 and Fig. 1a). Differently, the sample W-W_2C, prepared with larger addition of carbon (7.2 at.%) in the form of WC, is composed of W reinforced by 4 wt% W_2C. The third examined sample, WC—C, prepared from WC nanopowder with the addition of 2 at% of graphene (to prevent the formation of W_2C) [22–24], revealed the presence of free carbon in the WC matrix. The unreacted carbon remained in the form of aggregated graphene flakes, which can be seen in Fig. 1d (graphene flake is marked with an arrow).

The microstructure of the polished surface of W (Fig. 1b) shows pores (visible at the W grain boundaries as black features and marked with ellipses) in W-matrix. The W-W_2C composite and WC—C both exhibit denser bodies. From the XRD structural data (Fig. 1a) and SEM paired with EBSD analysis, we can assume that the W_2C phase in W-based samples inhibits W grain growth during powder consolidation. Namely, the average tungsten grain size in the W sample was determined to be 10.8 μm, while the average W grain size in the W-W_2C sample was 7.5 μm[25]. The role of W_2C as a W grain growth inhibitor was described in detail in a paper by Novak et al. [18]. In the case of WC—C, the grain size remains below one micron (average WC grain size was determined to be 0.6 μm) as in the starting powder. The latter can be attributed to FAST's rapid consolidation, which enables the densification of materials at no or with a minimum grain growth [26,27].

3.2. Deuterium retention

The measured depth profiles and desorption spectra for deuterium are shown in Fig. 2. The D depth profiles measured after both fluence exposures at 370 K and the high fluence exposure at 523 K are plotted in Fig. 3a-c with blue, black and red, respectively. The D desorption spectra were measured only for the high fluence samples exposed at 370 K and 450 K.

In Fig. 2a, we can see that the D depth profile for W is relatively homogeneous throughout the entire probing depth with a concentration equal to 0.05 at.% and 0.04 at.% for an exposure temperature of 370 K and 523 K, respectively, for the high fluence of 1.3×10^{25} D/m^2. A small but measurable difference in D concentration arises because, at higher

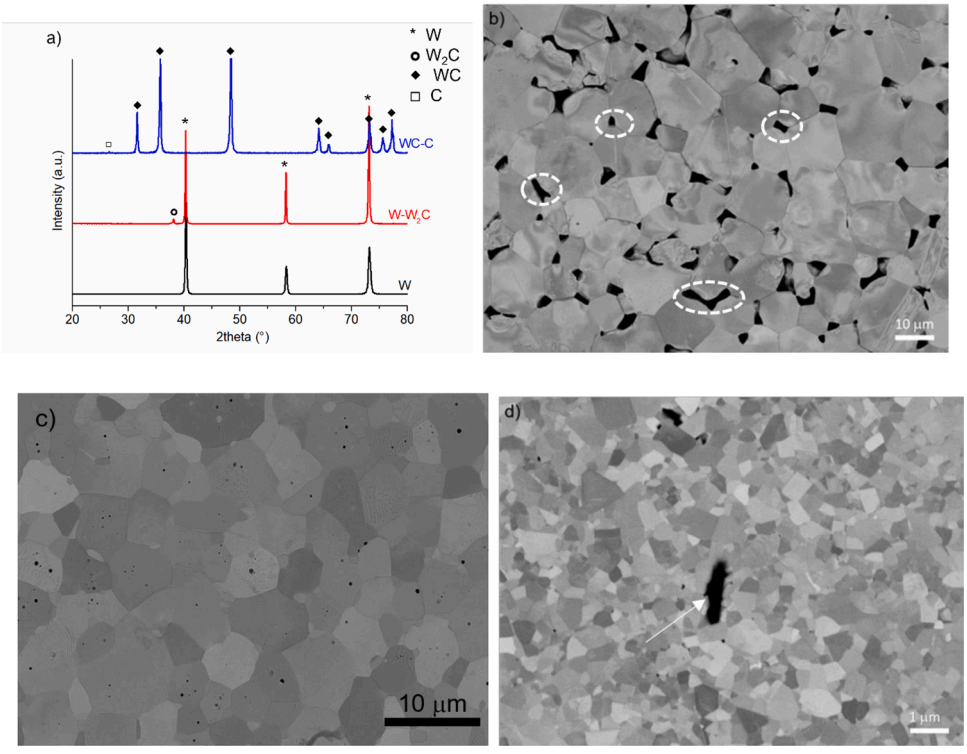

Fig. 1. a) XRD diffraction patterns of investigated samples and SEM-BSE micrographs of polished surfaces of as-consolidated pieces. b) W, c) W-W_2C, and d) WC-C (the arrow indicates unreacted carbon).

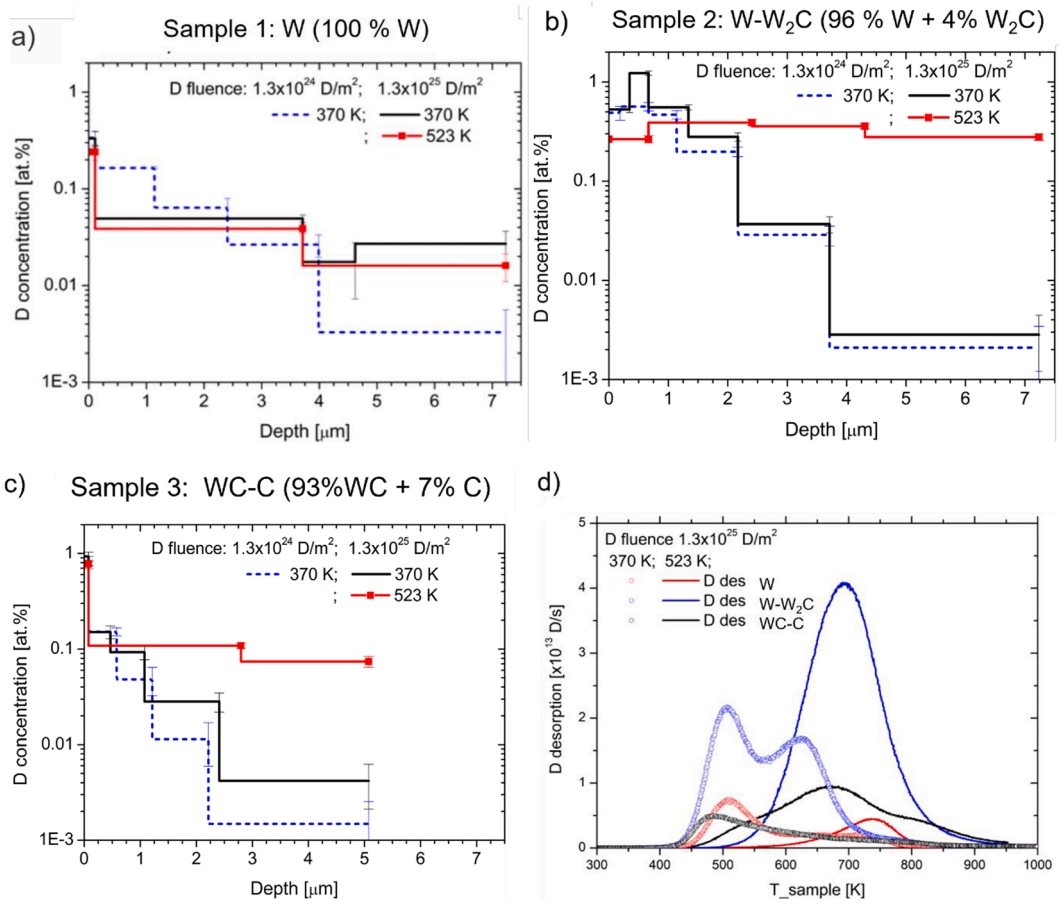

Fig. 2. Deuterium depth profiles and desorption spectra: a)-c) D depth profiles for all three samples for an exposure temperature of 370 K for two different fluences (dashed blue and black) and for an exposure temperature of 523 K (red); (d) the D desorption spectra for all three samples exposed at 370°K (circles) and 523°K (solid line).

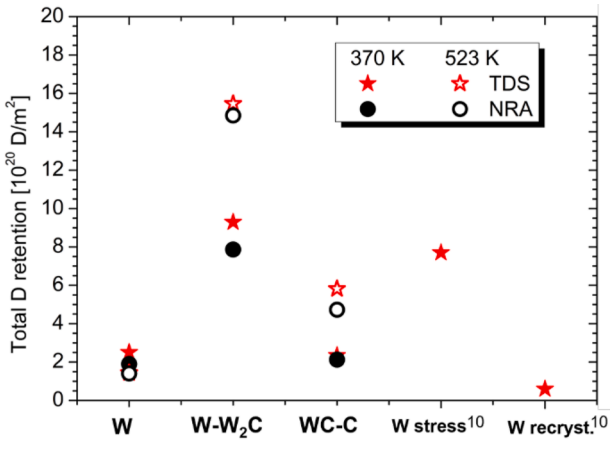

Fig. 3. Total D retention measured in the samples after exposure to a fluence of 1.3×10^{25} D/m^2 at 370 K and 523 K. The D retention is shown for NRA and TDS measurements as black circles and red stars, respectively. D retention is also shown for W produced by Plansee, where the material was before plasma exposure in one case heated to 1700 K (W stress) and in the other case heated to 2000 K (W recryst.) [10].

exposure temperatures, D de-trapping from lattice defects is more probable compared to lower exposure temperatures. A significant peak in the D depth profile is measured directly at the surface with a depth of 0.1 μm and a D concentration of approximately 0.3 at.% in both cases. Such a rise is often observed in D depth profile measurements and is usually attributed to D surface adsorption [28–30]. The D depth profile for the low fluence (1.3×10^{24} D/m^2) sample at 370 K shows a smaller penetration depth than the high fluence depth profile at the same temperature. This is due to the time dependence of the transport of deuterium atoms into depth. With D transport, we mean the combination of trapping and de-trapping in defects and diffusion, since when defects are present in a sample, the diffusion does not occur only through interstitial sites but also over substitutional sites where defects are present. However, the D concentration down to 4 μm depth is similar for both exposure fluences.

The D depth profiles of the W-W$_2$C composite are shown in Fig. 2b. The D depth profile measured after the 370 K exposure extends to only approximately 4 μm but has a much higher D concentration of roughly 0.5 at.% compared to a ten times lower concentration measured on the W sample. The higher D concentration indicates the presence of more lattice defects capable of retaining D compared to the W sample. The penetration depth for the two fluences at 370 K does not differ much. We see only a slight increase in D concentration with a longer exposure time. From the shallower depth of D penetration compared to W and slight increase with longer exposure time, i.e. fluence, we can infer that not all of the lattice defects in the probing depth could be saturated with D with the chosen D fluence. At an exposure temperature of 523 K, the D depth profile is more homogeneous and goes deeper but with a slightly lower average D concentration of 0.4 at.% compared to the 370 K case. Higher exposure temperature promotes D de-trapping and diffusion, thus making D transport faster with lower D concentration. The D concentration of 0.4 at.% is again ten times higher than the average D concentration measured in W.

The D depth profiles measured in WC—C for exposure fluences and temperatures show similar behaviour to the D depth profiles measured in the W-W_2C composite. At 370 K, the D has penetrated only to a depth of about 2.2 μm with a steeped D depth profile for the two exposure fluences with a slight increase in D concentration with a longer exposure time. The maximum concentration near the surface is 0.15 at.% which is higher than in the case of the W sample but lower than in the W-W_2C. At 523 K, the D depth profile is homogeneous down to analysing the depth of 5 μm with a concentration of 0.1 at.%, which is approximately two times higher than the D concentration measured in W and four times lower than in the case of W-W_2C.

The D desorption spectra of the samples exposed at 370 K and 523 K at a fluence of 1.3×10^{25} D/m^2 are shown in Fig. 2d. The D desorption starts at around 400 K for the 370 K set of samples, which is consistent with the exposure temperature. The D desorption has a significant peak at about 500 K in all three samples. In the case of W-W_2C, a second desorption peak is formed at 650 K, while the other two samples do not show this characteristic. Still, a long D desorption tail and shoulder are found in all three samples centred around 700 K, which extends D desorption up to a temperature of 850 K. The overall D desorption is the highest in W-W_2C, consistent with NRA's highest D concentration levels. The overall D desorption is similar in W and WC—C samples, even though a higher D concentration was measured in WC—C. The presented result implies that the D has penetrated beyond the NRA analysing depth in W. For the 523 K exposure temperature, the D desorption also starts close to the exposure temperature except for the WC—C sample, where desorption begins at about 450 K. In all cases, the main desorption signal shifts to the higher temperature of about 750 K for the W sample and 700 K for the W-W_2C and WC—C samples. The transition to higher temperatures could be due to deeper penetration depths for the W-W_2C and WC—C samples. In the W sample, D depth profiles were similar for both exposure temperatures, but the D desorption spectra were different. A high-temperature peak for the 523 K exposure is observed, which looked more like a tail in the 370 K case, and the low-temperature peak is diminished.

Finally, the cumulative D retention obtained by NRA and TDS in all three samples is shown for both D exposure temperatures in Fig. 4. The NRA D retention was calculated by summing up the area under the D depth profiles shown in Figs. 2a)-c). The TDS was obtained by summing the area under the desorption signal divided by the sample's surface area. We can observe that the agreement between NRA and TDS retentions is good. For W-W_2C and WC—C, the TDS retention is above the NRA retention meaning that D penetrated deeper into the material, as was the analysing depth of the NRA.

D retention is expected to fall with rising D exposure temperature because the probability of D de-trapping from the lattice defects in which it is captured rises with D exposure temperature. Such behaviour is observed in W, where NRA D retention is $(18.9 \pm 0.7)\ 10^{19}$ D/m^2 and $(14.1 \pm 0.5)\ 10^{19}$ D/m^2 for a D exposure temperature of 370 K and 523 K, respectively. In the other two samples, this generally valid behaviour is not observed. In the case of W-W_2C, NRA D retention is $(78.7 \pm 2.9)\ 10^{19}$ D/m^2 and $(148.4 \pm 1.5)\ 10^{19}$ D/m^2 for a D exposure temperature of 370 K and 523 K, respectively. In the case of WC—C, NRA D retentions are $(21.3 \pm 0.8)\ 10^{19}$ D/m^2 and $(47.2 \pm 1.1)\ 10^{19}$ D/m^2 for a D exposure temperature of 370 K and 523 K, respectively. For comparison, we also show D retention in W material produced by Plansee, purity 99.97%, where in one case, W material was before plasma exposure heated to 1700 K, the so-called stress-relieved material, marked as "W stress" and in the other case, W was heated to 2000 K which results in recrystallisation of W material, marked "W recryst" [10]. The D exposure was performed in the same plasma device at the same bias voltage and 370 K, with a D ion fluence of 6×10^{24} D/m^2. We compare our materials to Plansee W since this is the most often used material in the community and we take it here as a reference. The D retention in the W-W_2C samples is similar to the W Plansee, only stress-relieved, whereas the D retention in the other two samples is still high but closer to the W recrystallised. The higher D retentions measured at 523 K compared to the ones measured at 370 K can be explained by the fact that D had penetrated deeper into the samples when the exposure was done at a higher exposure temperature. We expect that if a larger D fluence were used during the D exposure, which would be sufficient to populate all defects up to our maximum NRA analysing depth of 7 μm, overall D retentions in all samples would fall with rising exposure temperature. This observation is important when extrapolating our D retention experimental results to possible future use of the investigated materials in tokamak reactors like EU DEMO.

After the D exposure and NRA analysis, samples were analysed by SEM to check if the D plasma exposure affected the surfaces' structure. The microstructural analysis after D exposure revealed the formation of blisters and pillars in samples W and W-W_2C but not in sample WC—C. The difference in the occurrence of blisters and pillars (marked with circles in Fig. 4) between samples W and W-W_2C is not evident at fluence 1.3×10^{24} D/m^2, but the contrast becomes apparent at the higher fluence. Namely, in the sample W-W_2C, approximately 15–20-times more blisters and pillars were formed than in W. Blisters are approx. 0.5—2 μm in diameter and 100—200 nm in height on both samples. A pronounced W grain orientation dependence can be observed after irradiation in the form of a spongy-like surface structure at certain grains, as previously reported by Xu et al. [31]. However, we cannot conclude that surface damage caused by the sample preparation influenced the formation of blisters since they formed in both damaged an un-damaged grain. The intrusion of hydrogen isotopes under high flux introduces

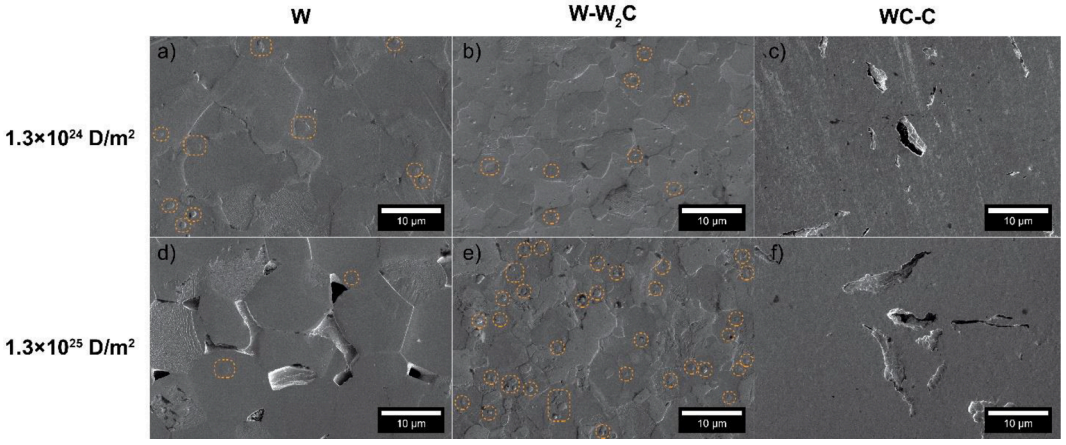

Fig. 4. The microstructural comparison between W, W-W_2C and WC—C samples, 1.3×10^{24} D/m^2 and 1.3×10^{25} D/m^2. The scale bar is 10 μm, and it is the same for all six figures.

crystal defects such as vacancies in the near-surface region [32]. Pillar formations after D irradiation have been previously described by Shu et al. [33]. They observed two types of blisters; high-dome blisters approximately 1 μm in diameter and larger ones which appeared flattered and were predominantly caused by voids and holes along the grain boundary beneath, but no hollow cover formed. In the case of our samples, the blisters never exceeded 2 μm in diameter and always retained a flat-dome shape. The cavity formation was also not specific to the microstructure features, such as grain boundary. Although more blisters and pillars were formed in the W-W_2C, we did not observe their formation of them on the W_2C grains. No irradiation defects were observed on the WC—C sample (Fig. 4c and f) apart from initial porosity due to graphene flake segregation at any temperature of fluence. Our experimental observations can be correlated with a recent paper by Salehin et al. [34] in which they were studying hydrogen trapping in transition metal oxides. They have found that the lower the carbon concentration, the more hydrogen the transition metal can store. Also, they have shown that VIB group of metal carbides (amongst which, both WC and W_2C are) are either weak, or do not trap hydrogen at al. So, if we correlate the formation of blisters and pillars with the phase composition and its capability to store hydrogen, then we can presume that tungsten carbides will be less likely to form blisters and pillars than pure tungsten.

A cross-section by focused ion beam (FIB) cut offers insight into blister morphology. Blisters on the W sample formed close to the surface, as shown in Fig. 5. The surface morphology of the blisters on samples W and W-W_2C are undistinguishable, but defects that result in blisters generally originate deeper within the W-W_2C sample, as represented in Fig. 5d. The height-to-diameter ratio of the cavities also varies considerably, from approximately 0.2 for W and 0.7 for W-W_2C samples, respectively. In the case of W, an elliptic-shaped cavity forms as a crack under the dome.

As mentioned above, plasma-induced surface modification was previously reported in rolled W and recrystallised W [31]. Here we show this is also the case in W and W-W_2C produced by FAST, although the materials' microstructure is quite different. From the total D retention study (Fig. 3), we can see that the higher concentration of defects is present in W-W_2C, followed by W stress (rolled W stress relieved at 1700 K), W (FAST) and W recryst. (rolled W-recrystallized). By introducing W_2C in W-matrix (Fig. 1), matrix grain-refinement was observed, caused by the formation of the W_2C phase but simultaneously, the amount of D trapping sites at microstructural features and defects increases [25]. Even if the grain size is further reduced and the material changes its nature from metal (W) through metal-based material (W-W_2C) to ceramic WC (WC—C), the overall amount of defects that can trap D is still high. Lasa et al. did molecular dynamics (MD) simulations on deuterium bombardment of W, WC and W_2C [35]. Their simulations showed that in WC and W_2C the trapped D is forming D_2 molecules, while in W D is mostly present in atomic form. They also suggest that the higher the C content (e.g. in WC) the formation of D_2 is promoted, while when there is lower C content present in the system (e.g. W_2C) carbon acts as a trapping centre for larger D_2 molecules. Later results in a relatively high D retention, which is in W-W_2C four times higher compared to W recrystallised.

Conclusions

Here the FAST consolidated W, W-W_2C composites and WC samples were examined in terms of D retention at D fluence of 1.3×10^{24} D/m^2 and 1.3×10^{25} D/m^2 at 370 K and 523 K. The results have shown that the lowest D retention was in sample W, where it retained (18.9 ± 0.7) 10^{19} D/m^2 and (14.1 ± 0.5) 10^{19} D/m^2 of D for a D exposure temperature of 370 K and 523 K, respectively. The second highest D retention was observed in the sample WC—C with D retention of (21.3 ± 0.8) 10^{19} D/m^2 and (47.2 ± 1.1) 10^{19} D/m^2 for a D exposure temperature of 370 K and 523 K. The highest D retention was displayed by the sample W-W_2C, in which W was reinforced by 4 wt% of W_2C, and it was (78.7 ± 2.9) 10^{19} D/m^2 and (148.4 ± 1.5) 10^{19} D/m^2 for a D exposure temperature of 370 K and 523 K, respectively. The microstructural examination revealed the formation of blisters and pillars in samples W and W-W_2C but not in sample WC—C. At the higher D fluence, approximately 15–20-times more blisters and pillars were formed in the sample W-W_2C than in sample W. Although there were more blisters and pillars formed in the W-W_2C composite than in pure W, there is no clear evidence that the tungsten carbides are trapping sites for hydrogen isotopes, mainly since

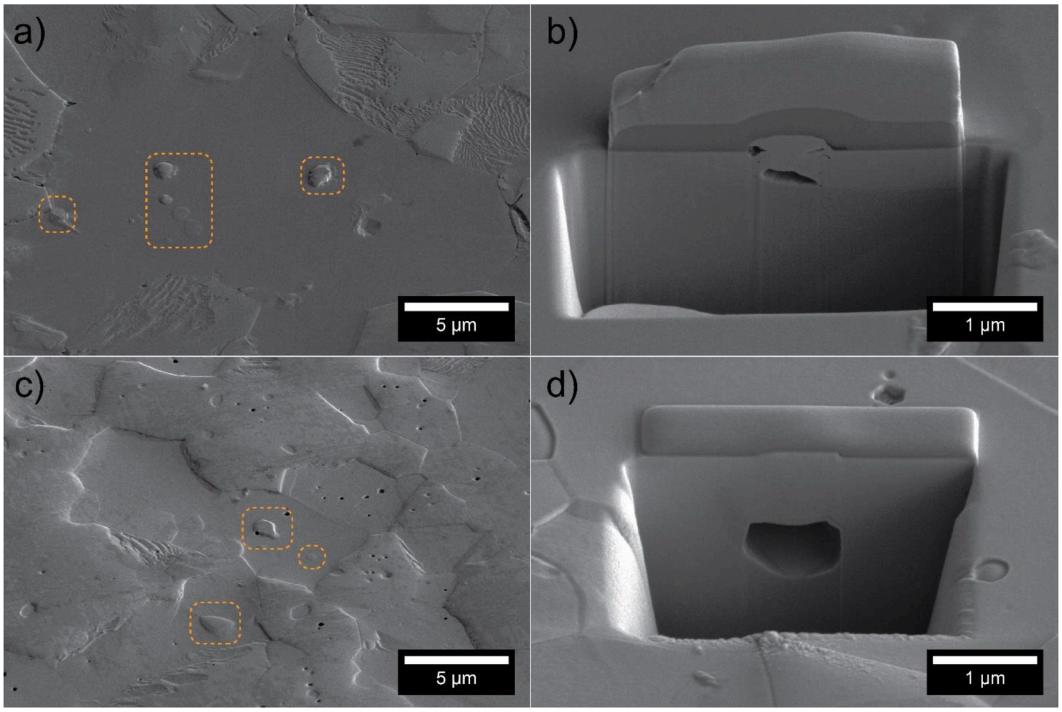

Fig. 5. Top-side (a and c) and cross-section (b and d) view of blisters and cavities on W (a and b) and W-W_2C (c and d) samples at fluence 1.3×10^{25} D/m^2.

no surface irregularities were observed in WC—C sample. The latter indicates that in the tungsten-tungsten carbide system, the microstructural and crystal lattice defects presumably govern the D retention.

CRediT authorship contribution statement

Petra Jenuš: Conceptualisation, Methodology, Project administration, Writing – original draft, Writing – review and editing, Visualization; **Anže Abram**: Investigation, Writing – original draft, Writing – review and editing; **Saša Novak**: Project administration, Supervision, Writing – review and editing, Funding acquisition; **Mitja Kelemen**: Resources, Investigation; **Matic Pečovnik**: Resources, Investigation, Data analysis; **Thomas Schwarz-Selinger**: Investigation, Writing – review and editing; **Sabina Markelj**: Methodology, Investigation, Writing – original draft, Writing – review and editing, Funding acquisition.

Declaration of competing interest

The authors declare that they have no known competing financial interests or personal relationships that could have appeared to influence the work reported in this paper.

Data availability

Data will be made available on request.

Acknowledgement

This work has been carried out within the framework of the EUROfusion Consortium, funded by the European Union via the Euratom Research and Training Programme (Grant Agreement No 101052200 — EUROfusion). Views and opinions expressed are however those of the author(s) only and do not necessarily reflect those of the European Union or the European Commission. Neither the European Union nor the European Commission can be held responsible for them. This project has received funding from the Slovenian Research Agency (Contracts No. 1000-17-0106, J2-8165, P2-0087-2 and P2-0405-5). The authors would like to thank Mr Matej Kocen for performing FAST sintering of samples and Ms Andreja Šestan Zavašnik for SEM analysis.

References

[1] M. Rieth, et al., Review on the EFDA programme on tungsten materials technology and science, J. Nucl. Mater. 417 (2011) 463–467.
[2] M. Rieth, et al., Recent progress in research on tungsten materials for nuclear fusion applications in Europe, J. Nucl. Mater. 432 (2013) 482–500.
[3] G. Pintsuk, Tungsten as a plasma-facing material, Comprehens. Nucl. Mater. 4 (2012).
[4] J. Roth, et al., Tritium inventory in ITER plasma-facing materials and tritium removal procedures, Plasma Phys. Control. Fusion 50 (2008).
[5] J.H. You, A review on two previous divertor target concepts for DEMO: mutual impact between structural design requirements and materials performance, Nucl. Fusion 55 (2015).
[6] Y. Hatano, et al., Deuterium trapping at defects created with neutron and ion irradiations in tungsten, Nucl. Fusion 53 (2013).
[7] E. Lassner, W.-.D. Schubert, The Element Tungsten, Tungsten (1999) 1–59, https://doi.org/10.1007/978-1-4615-4907-9_1.
[8] Waseem, O.A. & Ryu, H.J. Tungsten-based composites for nuclear fusion applications.
[9] S. Antusch, J. Reiser, J. Hoffmann, A. Onea, Refractory materials for energy applications, Energy Technol. 5 (2017) 1064–1070.
[10] A. Manhard, K. Schmid, M. Balden, W Jacob, Influence of the microstructure on the deuterium retention in tungsten, J. Nucl. Mater. 415 (2011) S632–S635.
[11] P. Norajitra, Divertor Development for a Future Fusion Power Plant, KIT Scientific Publishing, 2014.
[12] G.-.M. Song, Y.-.J. Wang, Y Zhou, Thermomechanical properties of TiC particle-reinforced tungsten composites for high temperature applications, Int. J. Refract. Met. Hard Mater. 21 (2003) 1–12.
[13] L. Huang, et al., In situ oxide dispersion strengthened tungsten alloys with high compressive strength and high strain-to-failure, Acta Mater 122 (2017) 19–31.
[14] X.-.Y. Tan, et al., Development of tungsten as plasma-facing materials by doping tantalum carbide nanoparticles, Powder Technol 269 (2015) 437–442.
[15] Y. Kitsunai, et al., Microstructure and impact properties of ultra-fine grained tungsten alloys dispersed with TiC, J. Nucl. Mater. 271 (1999) 423–428.
[16] S. Lang, et al., Preparation and microstructure characterization of W–0.1wt.%TiC alloy via chemical method, Int. J. Refract. Met. Hard Mater. 55 (2016) 33–38.
[17] P. Jenuš, A. Iveković, M. Kocen, A. Šestan, S. Novak, W2C-reinforced tungsten prepared using different precursors, Ceram. Int. (2018), https://doi.org/10.1016/j.ceramint.2018.11.187.
[18] S. Novak, et al., Beneficial effects of a WC addition in FAST-densified tungsten, Mater. Sci. Eng. A 772 (2020), 138666.
[19] E. Salançon, T. Dürbeck, T. Schwarz-Selinger, F. Genoese, W Jacob, Redeposition of amorphous hydrogenated carbon films during thermal decomposition, J. Nucl. Mater. 376 (2008) 160–168.
[20] K. Schmid, U Von Toussaint, Statistically sound evaluation of trace element depth profiles by ion beam analysis, Nucl. Instruments Methods Phys. Res. Sect. B Beam Interact. with Mater. Atoms (2012), https://doi.org/10.1016/j.nimb.2012.03.024.
[21] T. Schwarz-Selinger, J. Bauer, S. Elgeti, S. Markelj, Influence of the presence of deuterium on displacement damage in tungsten, Nucl. Mater. Energy 17 (2018) 228–234.
[22] J. Sun, et al., A review on binderless tungsten carbide: development and application, Nano-Micro Letters 12 (2020).
[23] C.P. Buhsmer, P.H Crayton, Carbon self-diffusion in tungsten carbide, J. Mater. Sci. 6 (1971) 981–988.
[24] Z.Z. Fang, X. Wang, T. Ryu, K.S. Hwang, H.Y. Sohn, Synthesis, sintering, and mechanical properties of nanocrystalline cemented tungsten carbide – A review, Int. J. Refract. Met. Hard Mater. 27 (2009) 288–299.
[25] A. Šestan, et al., Non-uniform He bubble formation in W/W2C composite: experimental and ab-initio study, Acta Mater 226 (2022), 117608.
[26] Z.A. Munir, U. Anselmi-Tamburini, M. Ohyanagi, The effect of electric field and pressure on the synthesis and consolidation of materials: a review of the spark plasma sintering method, J. Mater. Sci. 41 (2006) 763–777.
[27] Kirchner, R. *"FAST " - Field Assisted Sintering Technology Basics , State of the Art and Future Aspects.* (2011).
[28] S. Markelj, et al., Displacement damage stabilization by hydrogen presence under simultaneous W ion damage and D ion exposure, Nucl. Fusion 59 (2019).
[29] S. Markelj, et al., Deuterium retention in tungsten simultaneously damaged by high energy W ions and loaded by D atoms, Nucl. Mater. Energy 12 (2017) 169–174.
[30] M. Pečovnik, E.A. Hodille, T. Schwarz-Selinger, C. Grisolia, S. Markelj, New rate equation model to describe the stabilization of displacement damage by hydrogen atoms during ion irradiation in tungsten, Nucl. Fusion 60 (2020), 036024.
[31] H.Y. Xu, et al., Observations of orientation dependence of surface morphology in tungsten implanted by low energy and high flux D plasma, J. Nucl. Mater. 443 (2013) 452–457.
[32] W.M. Shu, G.N. Luo, T. Yamanishi, Mechanisms of retention and blistering in near-surface region of tungsten exposed to high flux deuterium plasmas of tens of eV, J. Nucl. Mater. 367-370 B (2007) 1463–1467.
[33] W.M. Shu, A. Kawasuso, T. Yamanishi, Recent findings on blistering and deuterium retention in tungsten exposed to high-fluence deuterium plasma, J. Nucl. Mater. 386–388 (2009) 356–359.
[34] R. Salehin, G.B. Thompson, C.R Weinberger, Hydrogen trapping and storage in the group IVB-VIB transition metal carbides, Mater. Des. 214 (2022), 110399.
[35] A. Lasa, C. Björkas, K. Vörtler, K. Nordlund, MD simulations of low energy deuterium irradiation on W, WC and W2C surfaces, J. Nucl. Mater. 429 (2012) 284–292.